

# Lattice Boltzmann simulations of sound directivity of a cylindrical pipe with mean flow

Yong Shi<sup>1)</sup>, Andrey R. da Silva<sup>2)</sup>, Gary P. Scavone<sup>1)</sup>

<sup>1)</sup> Computational Acoustic Modeling Laboratory and Centre for Interdisciplinary Research in Music Media and Technology, Schulich School of Music, McGill University, Montreal, Quebec, Canada.

yong.shi2@mail.mcgill.ca, gary.scavone@mcgill.ca

<sup>2)</sup> Center for Mobility Engineering, Federal University of Santa Catarina, Joinville, Brazil. andrey.rs@ufsc.br

**Abstract.** This paper proposes a numerical scheme based on the lattice Boltzmann method to tackle the classical problem of sound radiation directivity of pipes issuing subsonic mean flows. The investigation is focused on normal mode radiation, which allows the use of a two-dimensional lattice with an axisymmetric condition at the pipe's longitudinal axis. The numerical results are initially verified against an exact analytical solution for the sound radiation directivity of an unflanged pipe in the absence of a mean flow, which shows a very good agreement. Thereafter, the sound directivity results in the presence of a subsonic mean flow are compared with both analytical models and experimental data. The results are in good agreement, particularly for low values of the Helmholtz number  $ka$ . Moreover, the phenomenon known as 'zone of relative silence' was observed, even for mean flows associated with very low Mach numbers, though discrepancies were also observed in the comparison between the numerical results and the analytical predictions. A thorough discussion on the scheme implementation and numerical results is provided in the paper.

## 1. Introduction

The mechanisms of sound radiation from the open end of ducts have been investigated by many researches over the last century and remains an important problem in acoustics. Among all the sound radiation parameters, the acoustic directivity, which is a measure of the angular distribution of acoustic energy around the sound source, is paramount to defining strategies for noise control in systems such as exhaust pipes, jet engines, ventilation systems and so on.

Nevertheless, exact analytical solutions for the directivity problem are only available for very simple geometries (cylindrical and annular pipes) and low compressibility regimes. In realistic situations involving real outlet systems, the geometrical characteristics and flow conditions differ considerably from the conditions imposed by available analytical models. For such cases, numerical techniques provide essential tools for addressing the problem.

The first exact analytical model for the sound directivity from cylindrical pipes was proposed by Levine and Schwinger [1], based on the Wiener-Hopf technique. The solution is limited to normal mode propagation (plane waves) and assumes a stagnant mean flow. Munt [2] extended this model by considering the presence of a low-Mach number mean flow. In his solution, a full Kutta condition is imposed at the edges of the pipe, the mean flow is assumed to be uniform (plug) and the vortex sheet separating the jet and the outer fluid is considered infinitely thin. The solution is exact, provided that the Helmholtz number  $ka < 1.5$  and the Mach number  $M < 0.3$ . Rienstra [3] improved Munt's solution by introducing a complex parameter to take into account the effects of unsteady vortex shedding in the vicinity of the trailing edge, with particular attention to the energy balance between the sound and the fluid fields. Based on the work of both Munt and Rienstra, Gabard and Astley [4] presented an extended model that includes a center body for the cases of annular pipe and proposed an explicit numerical procedure for evaluating the solutions for higher frequencies and higher compressibility regimes ( $0 < ka < 60$  and  $0 < M < 0.8$ ).

Numerical techniques have also been used to tackle problems of sound radiation directivity of ducts involving more complex conditions. For example, Rumsey et al. [5] analyzed the generation and propagation of unsteady duct acoustic modes resulting from a rotor-stator interaction in a 3D configuration by using a Navier-Stokes numerical simulation. Zhang et al. [6] modeled the sound radiation from an unflanged duct of aircraft engines through linearized Euler equation (LEE) solutions. Ozyoruk et al. [7] predicted the sound fields of ducted fans carrying an axisymmetric non-uniform background flow by solving the LEE. Chen et al. [8] analyzed the planar wave radiation from an unflanged duct by solving the LEE. More recently, Hornikx et al. [9] presented a numerical solution for calculating the sound field radiated from an automotive exhaust pipe situated over a rigid surface. The mean flow was represented by Reynolds averaged Navier-Stokes equations (RANS) and the sound field represented by the linearized Euler equations, which were resolved with the Fourier pseudo-spectral time domain technique

(PSTD).

When compared to traditional numerical techniques, there has been less investigation on the use of the lattice Boltzmann method (LBM) to solve acoustic problems, though several interesting studies have been reported. For example, Buick et al. [10] [11] investigated sound waves in an unbound fluid using a two-dimensional lattice Boltzmann scheme with a Bhatnagar-Gross-Krook (BGK) approximation [12]). Later on, Buick et al. investigated the jet formation at a pipe end [13]. Viggen [14] investigated the effects of viscosity on spatially damped acoustic waves using the BGK scheme. More recently, Viggen [15] implemented acoustic multipole sources in an acoustic field with zero viscosity in the LBM scheme by including a source term and using a regularized collision operator. In aeroacoustic problems involving the interaction between the flow and the acoustic fields, Li et al. [16] simulated wave propagations in the presence of compressible flow regimes. Kam et al. [17] simulated the scattering of acoustic waves and Li and Shan [18] proposed a LBM scheme for adiabatic acoustic phenomena. Lew and Mongeau [19] simulated the axisymmetric subsonic turbulent cold jet issuing from a pipe and its influence on sound radiation. Subsequently, Habibi et al. [20] added a heat transfer model to the LBM scheme to study heated jets. In the specific case of sound radiation from the open end of ducts, da Silva and Scavone [21] investigated the sound radiation from an unflanged cylinder immersed in a stagnant fluid in terms of the sound reflection coefficient  $R$  and the radiation directivity. Later, they investigated the influence of a subsonic mean flow on the sound reflection coefficient of ducts terminated by horns with different geometries [22]. The results agreed well with the analytical theory proposed by Munt [23] and the experimental data obtained by Peters et al. [24] and Allam and Åbom [25].

The objective of this paper is to use the LBM to address the problem of sound directivity of ducts issuing a subsonic mean flow. The problem conditions will be limited to the radiation of normal (planar) modes and low compressibility regimes. For this reason, the numerical scheme used in this paper is based on an isothermal model represented in a two-dimensional axisymmetric scheme.

This paper is structured as follows: Section 2 describes the numerical technique used in the study. In Section 3, the simulation results for an unflanged pipe are compared to the analytical model by Levine and Schwinger [1] and the experimental data obtained by Gorazd et al. [26], for the case of zero mean flow. The directivity results obtained when considering a subsonic mean flow are compared with the analytical results from Gabard and Astley [4] and with the experimental results by Gorazd et al. [26]. Moreover, the phenomenon associated with the zone of relative silence observed in the simulations is discussed. Finally, Section 4 provides a discussion of the results and suggestions for further investigations.

## 2. Numerical Procedure

The fluid/aeroacoustic system in this study is characterized by a 3D axisymmetric flow in an unflanged cylindrical pipe. Although it is possible to simulate the 3D flow using a 3D LBGK model, this approach would require significant computational resources (CPU time, memory, etc.). Rather, an axisymmetric 2D LBGK scheme is chosen for its efficiency and simplicity. Halliday et al. [27] first proposed an axisymmetric model for the steady 3D axisymmetric tube flow problems, where they inserted several spatial and velocity-dependent source terms into the RHS of the collision equation of a regular LBGK D2Q9 model ‡, such that the Navier-Stokes equations in cylindrical polar coordinates can be recovered from the lattice Boltzmann equation by performing a Chapman-Enskog expansion. Later Niu et al. [29] derived an axisymmetric model for the Taylor-Couette flow problems. Lee et al. [30] further proposed an axisymmetric scheme based on the incompressible LBGK D2Q9 model [31] for simulations of 3D pulsatile flow.

In our study, the axisymmetric incompressible LBGK D2Q9 model by Lee et al. [30] was employed to simulate the 3D axisymmetric flow in a circular pipe. This scheme assumes that the flow is symmetric about the pipe's axis and thus can be expressed by the incompressible Navier-Stokes equations in cylindrical polar coordinates. Based on this assumption, the azimuthal component of velocity  $u_\phi$  and the  $\phi$  coordinate derivatives vanish. Consequently, the flow can be represented by the axial and radial coordinates,  $x$  and  $r$ , respectively. The adapted Boltzmann equation uses the BGK approximation with a simple scalar relaxation time  $\tau$  for the collision function. The two main steps of collision and streaming are represented by

$$f_i(x + c_{ix}, r + c_{ir}, t + 1) - f_i(x, r, t) = -\frac{1}{\tau}[f_i(x, r, t) - f_i^E(x, r, t)] + h_i^{(1)} + h_i^{(2)}, \quad (1)$$

where  $f_i$  is the distribution function for particles with velocity  $c_i$  at position  $(x, r)$  and time  $t$  and  $i = 0, 1, 2, \dots, 8$  indicates the site number associated with the propagation direction. The LHS of Eq. 1 is a convection operator describing the diffusion of the distribution function  $f_i$  over the lattice grid. The first term on the RHS of Eq. 1 refers to the intermolecular collision described by the relaxation time  $\tau$ , which determines the viscosity of the fluid by the relation  $\nu = \frac{2\tau-1}{6}$ . The equilibrium distribution function  $f^E$  is identical to that of an incompressible LBGK D2Q9 model [31] [30] given by

$$f_i^E(x, r, t) = \omega_i \frac{(\rho_0 + \delta\rho)}{c_s^2} + \omega_i \rho_0 \left[ \frac{\mathbf{c}_i \cdot \mathbf{u}}{c_s^2} + \frac{(\mathbf{c}_i \cdot \mathbf{u})^2}{2c_s^4} - \frac{\mathbf{u}^2}{2c_s^2} \right], \quad (2)$$

where  $\mathbf{c}_i$  is the discrete velocity connecting each site to its neighbor lattices,  $\omega_0 = 4/9$ ,  $\omega_1 = \omega_2 = \omega_3 = \omega_4 = 1/9$  and  $\omega_5 = \omega_6 = \omega_7 = \omega_8 = 1/36$  and  $c_s = 1/\sqrt{3}$  is the speed of sound.

‡ Here we follow the standard DdQn nomenclature proposed by Qian et al. [28]

The source terms on the RHS of Eq. (1) are given by

$$h_i^{(1)} = -\frac{\omega_i \rho_0 u_r}{r} \quad (3)$$

$$h_i^{(2)} = \omega_i \frac{3\nu}{r} [\partial_r p + \rho_0 \partial_x u_x u_r + \rho_0 \partial_r u_r u_r + \rho_0 (\partial_r u_x - \partial_x u_r) c_{ix}] \quad (4)$$

The velocity derivation terms  $\partial_r u_r$ ,  $\partial_x u_x$  and  $\partial_r u_x - \partial_x u_r$  in Eq. (4) can be solved using the technique proposed by Lee et al. [30]. Specifically, the terms  $\partial_r u_r$ ,  $\partial_x u_x$  and  $\partial_r u_x + \partial_x u_r$  are explicitly calculated from the higher-order moments of  $f_i$  by Eq. (9) in [30]. The term  $\partial_r u_x - \partial_x u_r$  is equal to  $\partial_r u_x + \partial_x u_r - 2\partial_x u_r$ , where the unknown term  $\partial_x u_r$  can be calculated using the finite difference method described by Eq. (10) in [30].

The macroscopic fluid density  $\rho$  and velocity  $u$  are expressed by the moments of the local distribution function  $f_i$  by

$$\rho(x, r, t) = \sum_i f_i(x, r, t), \quad (5)$$

$$\mathbf{u}(x, r, t) = \sum_i f_i(x, r, t) \mathbf{c}_i / \rho(x, r, t). \quad (6)$$

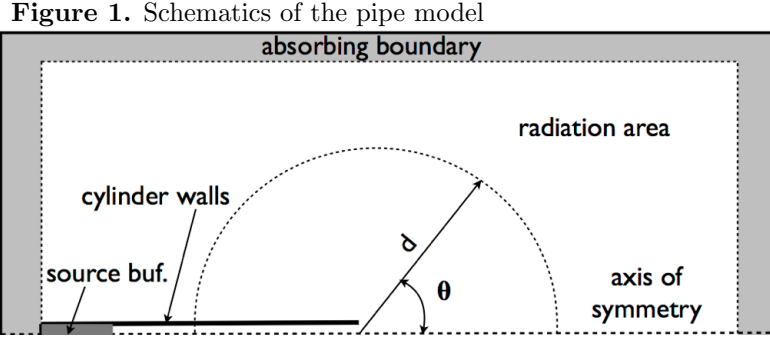
In the isothermal condition, the fluid pressure  $p$  is related to the fluid density and the speed of sound by

$$p = \rho c_s^2. \quad (7)$$

According to previous experiments, we have noticed that the axisymmetric model derived by Lee provides accurate results and offers a simpler numerical implementation. Generally speaking, an incompressible LBGK model is able to capture acoustic wave phenomena, provided that these are within the linear regimes characterized by low Mach numbers and low wave amplitudes. The highest Mach number used in this paper is  $M = 0.15$ , which makes the flow slightly compressible. However, the incompressible model is still valid because the slightly unsteady compressible form of the Navier-Stokes equations can be fully recovered from the isothermal form of the Boltzmann equation by performing the Chapman-Enskog expansion, as described in [28] and [32].

### 2.1. Pipe Model and Boundary Conditions

The purpose of the pipe model presented here is to capture the sound radiation directivity, which is the distribution of acoustic energy as a function of the angle measured about the pipe main axis for plane wave radiation. The pipe model is described by an axisymmetric cylinder structure immersed in a fluid domain surrounded by open boundaries, as illustrated in Fig. 2.1. The axisymmetry is exploited such that the system can be fully represented by a half-plane without losing accuracy. The fluid domain defined by the half-plane is represented by a rectangular D2Q9 structure of 1000 by 500 lattice cells.



The top, left and right side of the fluid domain are treated with an absorbing boundary condition (ABC) proposed by Kam et al. [33], which is a transition buffer with a target flow prescribed at the outlet. The non-reflecting condition is achieved by setting the distribution function of the target flow,  $f_i^T$ , to the equilibrium state, i.e.,  $\rho_t = \rho_0$  and  $u_t = 0$ , where  $\rho_0$  is the undisturbed density of the fluid. For collisions inside the transition buffer, an extra damping term is added to the collision equation of the single relaxation time BGK lattice Boltzmann scheme, as described in Eq. 8,

$$f_i(x + c_{ix}, r + c_{ir}, t + 1) - f_i(x, r, t) = -\frac{1}{\tau} [f_i(x, r, t) - f_i^E(x, r, t)] + h_i^{(1)} + h_i^{(2)} - \sigma(f_i^E - f_i^T) \quad (8)$$

where  $\sigma = \sigma_m(\delta/D)^2$  is the damping coefficient,  $\sigma_m$  is a constant, normally equals to 0.3,  $\delta$  is the distance measured from the beginning of the buffer zone and  $D$  is the thickness of the buffer. Inside the transition buffer, the amplitude of outgoing waves is attenuated asymptotically and the reflections from the outside boundary are minimized. The thickness of the ABC buffer used in the model is 30 cells, corresponding to a frequency-averaged pressure reflection coefficient of order of magnitude smaller than  $10^{-3}$  for both perpendicular and oblique sound incidence. The lower boundary of the radiation domain representing the axis of symmetry of the system is treated with a free-slip condition.

The length and the radius of the cylindrical waveguide is  $L = 469.5$  and  $a = 10$  in lattice cells, respectively. The walls of the waveguide are represented by a solid boundary of zero thickness based on spatial interpolations [34, 35]. The outer walls are treated by a simple bounce-back scheme [36] for which the viscous boundary phenomena are represented with second-order accuracy, while the inner walls are treated using a free-slip scheme described in [32], in order to reduce the inherent viscous boundary layer effects that result in a transfer of momentum by the tangential motion of particles along the walls.

The undisturbed dimensionless fluid density was set as  $\rho_0 = 1.0$  for convenience. To ensure the numerical stability and to make the viscosity as small as possible, the relaxation time is set to  $\tau = 0.5714$ , which is equivalent to a dimensionless viscosity of  $\nu = 0.0238$ . In fact, due to the BGK limitations, the viscosity asserted is one order of magnitude higher than that of air in normal conditions. A higher viscosity

could result in two significant effects: 1). Accentuated wave dissipation, particularly at higher frequency components, and 2). Spurious directivity artifact caused by the interaction between the viscous boundary layer and the rim of the pipe. In fact, if the viscosity is relatively high, the pipe can be seen as a capillary tube, where the radiation directivity is dominated by viscous phenomena. These effects are significantly minimized by measuring sound pressures at positions sufficiently close to the sound source (open end) and imposing a free-slip condition at the pipe wall. This last boundary condition is in accordance with the exact model from Munt [2], which is inviscid and the singularity at the sharp edge of the pipe is treated with a full Kutta condition.

The system is excited by a source signal that consists of a linear chirp signal running from  $ka = 0.1$  to  $ka = 3.8$  (less than the first evanescent mode of the pipe) superimposed on a DC offset representing the non-zero mean flow. The excitation is implemented by a source buffer with a length of 60 cells at the left end of the pipe using the same technique of an absorbing boundary conditions but prescribed by a non-zero target velocity given by

$$u_t = u_0 + H(n - N_t)u'_0 \sin \left[ \frac{c_s}{a} \left( 0.1 + 3.8 \frac{(n - N_t)\Delta t}{N - N_t} \right) \right], \quad (9)$$

where  $n$  is the time step,  $N$  is the total number of iterations in the simulation,  $N_t$  is the initialization iterations,  $u_0$  is the velocity of the non-zero mean flow,  $u'_0$  is the amplitude of the acoustic particle velocity along the axial direction and  $\Delta t = 1$  is the time increment of the numerical scheme.  $H(n)$  is the Heaviside step function given by

$$H(n) = \begin{cases} 0, & n < 0, \\ 1, & n \geq 0. \end{cases} \quad (10)$$

Before the acoustic source is superimposed, there should be enough initialization time to allow the fluid in the whole domain to accelerate from stagnation to a steady state. The initialization steps can be approximated by

$$N_t \geq N_{t0} + L_x/(Mc_s), \quad (11)$$

where  $N_{t0} = 4000$  is the acceleration time for the source buffer with thickness equivalent to 60 cells [22],  $M$  is the Mach number of the non-zero mean flow and  $L_x = 1000$  is the maximum traveling distance of the plane sound wave in the axial direction in the radiation domain. For example, the minimum initialization steps corresponding to a Mach number of  $M = 0.036$  is  $N_t = 5.21 \times 10^4$ .

The time histories of fluid density are probed at 75 points evenly distributed around the semi-circle (corresponding to angle increments of 2 degrees), with the center point at the outlet of the duct in the range of  $\theta = 0^\circ$  to  $\theta = 150^\circ$ . The measuring distance is  $d = 250$  cells from the outlet. The acoustic pressure  $p'$  is calculated by

$$p'(\theta, t) = (\rho(\theta, t) - \rho_0)c_s^2, \quad (12)$$

where  $\rho(\theta, t)$  is the spontaneous fluid density and  $\rho_0$  is the equilibrium density. For the case of zero mean flow,  $\rho_0$  is nearly a constant and usually has the value of 1. For non-zero mean flow, however,  $\rho_0$  in the vicinity of the probing points fluctuates over time and the fluctuating density can not be calculated by simply subtracting the stagnant field density (a value of 1) from the spontaneous fluid density. For such a case, a zero-phase DC-blocking filter can be used to remove the offset caused by the flow.

Once the time history of acoustic pressures has been obtained, the pressure directivity as a function of angle  $\theta$  and frequency  $f$  can be calculated by

$$G(\theta, f) = \frac{P(\theta, f)}{P_h}, \quad (13)$$

where  $P(\theta, f)$  is obtained by performing a DFT on the time history of sound pressure  $p'(\theta, t)$  measured at the same distance  $d$  and  $P_h = \sqrt{\sum P^2(\theta)/N}$  is the square root of the averaged value of  $P^2(\theta, f)$  over all the measured angles.

### 3. Results

#### 3.1. Directivity in the absence of mean flow

The LBM scheme in the absence of mean flow is first validated by comparing its results with the established analytical model proposed by Levine and Schwinger [1] in the form of relative pressure directivity. For six different frequencies expressed in terms of the Helmholtz number ( $ka = 0.48, 1, 2, 2.5, 3, 3.5$ ) that are below the cut-on frequencies of higher-order modes, the numerical simulations are in good agreement with the analytical results, as shown in Fig. 2. The tiny ripples found for  $ka = 0.48$  and  $ka = 1$  in the numerical results can be explained by the fact that  $G(\theta)$  should be measured in the far-field condition, which is not fully satisfied for low frequencies given the size of the lattice ( $1000 \times 500$  cells) and the measuring radius (250 cells) used in this paper (due to computation time limits). Not surprisingly, the results for higher frequencies ( $ka \geq 2$ ) are smooth and the ripples are barely observed. To evaluate the far-field condition in this simulation, we measured the acoustic impedance  $Z = P/U$  as a function of  $ka$  at a distance  $d = 250$  and angle  $\phi = 0$  from the outlet of the pipe, where  $P$  and  $U$  are obtained by performing an FFT to the time history of acoustic pressure  $p$  and particle velocity  $u$ , respectively. As depicted in Fig. 3(a), the amplitude of the impedance  $Z$  quickly approaches to the characteristic impedance of the medium,  $Z_c = \rho_0 c_s$ , for values of  $ka \geq 1$ . A similar phenomenon can be found for the phase between the acoustic pressure and particle velocity,  $\phi$ , which gradually approaches to zero for  $ka \geq 2$ , as depicted in Fig. 3(b). It is worth mentioning that the phase and the characteristic impedance will never converge completely to zero and  $\rho c$ , respectively, due to the viscous nature of the fluid [14]. The results suggest that the far-field condition is not fully satisfied for  $ka < 1$ , while for  $ka \geq 1$ , the acoustic impedance  $Z$  of the spherical wave propagating into the radiation domain approximates that of a plane wave.

The results of Fig. 2 show discrepancies at high angles (more obvious for  $\theta > 100^\circ$ ). We believe that these errors could come from the high viscosity in the simulation. Perhaps the viscosity affects the directivity of sound radiation or the viscous boundary layer on the outside of the pipe affects the results.

From Fig. 2(f), we can observe smoothing of directivity characteristics of numerical results in the vicinity of  $\theta = 100^\circ$  compared to that of the analytical results for the high frequency  $ka = 3.5$ . That might be attributed to the issue that, in the numerical simulation, there may be some transfer of energy from the exciting chirp signal to higher-order modes, while for the case of the analytical model, no higher modes are involved and the energies are exclusively coming from the dominant plane mode. More specifically, the exact analytical model derived by Levine and Schwinger only takes into account the directivity due to plane mode propagation up to  $ka = 3.82$ . While our source acts like a piston, it is possible that energy might be transferred to higher-order modes (via mode-coupling) near structural discontinuities, either in the form of evanescent or perhaps even propagating waves. Due to the shortness of the pipe, some of the energy associated with these higher modes may find its way out of the pipe. A similar phenomenon was reported in a recent experimental measurement conducted by Gorazd et al. [26], where the curves presenting the directivity characteristics of the experimental results (excited by broadband noise) around  $\theta = 100^\circ$  and for higher frequencies ( $ka \geq 2.96$ ) are smoothed compared to those analytical results obtained for a single-frequency exciting signal.

In the next step, the numerical and analytical results are compared with the experimental results by Gorazd et al. [26] in the form of relative pressure directivity. All three results (numerical, analytical and experimental) have been normalized to the same dB level, as depicted in Fig. 4. For the two lower frequencies of  $ka = 0.74$  and  $1.48$  and for angles within the range of  $0^\circ < \theta < 90^\circ$ , the three results are in good agreement with each other, despite the fact that the measurements are carried out using 1/3 octave broadband noise and the calculation of numerical and analytical results are based on a single frequency. As the angle increases, the measurements are still in good agreement with the analytical results, though the numerical results have discrepancies less than 3 dB compared to the analytical results. For the higher frequency of  $ka = 2.96$ , the numerical results are in good agreements with both the analytical results and the measurements for angles within the range of  $0^\circ < \theta < 75^\circ$ . As the angle increases from  $75^\circ$  to  $150^\circ$ , both the measurements and the numerical results deviate from the analytical results, but in opposite ways. Compared to the analytical results, the highest discrepancies are found at the largest angle of  $\theta = 150^\circ$ , which is +3.8 dB for the measurements and -2.6 dB for the numerical results, respectively.

### 3.2. Directivity in the presence of mean flow

For the case of a cold mean flow (i.e., the temperature gradient between the jet and the outer stagnant flow is zero) with a low Mach number ( $M = 0.036$ ), the numerical results

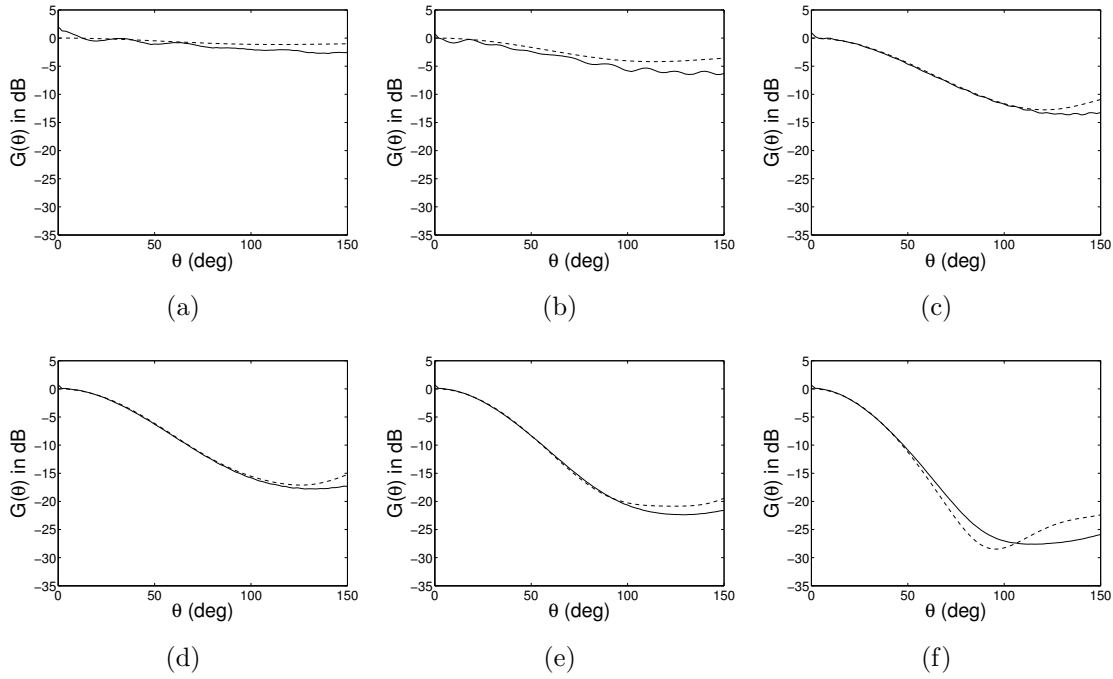


**Figure 2.** Comparison between numerical (solid) and analytical predictions [1] (---) of the acoustic pressure directivity as a function of the angle in the absence of a mean flow: (a)  $ka = 0.48$ , (b)  $ka = 1$ , (c)  $ka = 2$ , (d)  $ka = 2.5$ , (e)  $ka = 3$ , (f)  $ka = 3.5$ .

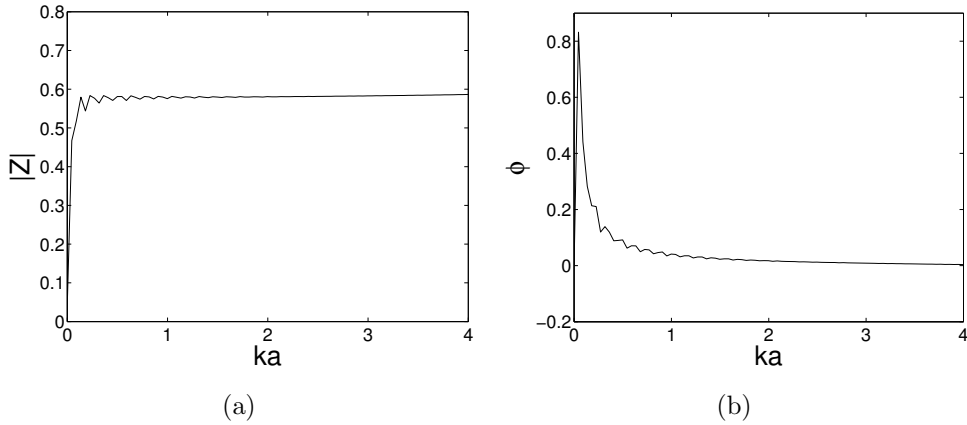


**Figure 3.** Evaluation of the far-field condition in terms of acoustic impedance in the radiation domain: (a) amplitude of acoustic impedance, (b) phase of acoustic impedance.

are compared with the theoretical prediction given by Gabard and Astley [4] as well as the recent experimental results obtained by Gorazd et al. [26] in the form of normalized pressure directivity, as depicted in Fig. 5. All three results (numerical, analytical and experimental) have been represented in the form of pressure directivity and normalized to the same dB level.

In general, the results are in good agreement for angles in the range  $0^\circ < \theta < 60^\circ$ . Discrepancies between the numerical and analytical results become more obvious as the

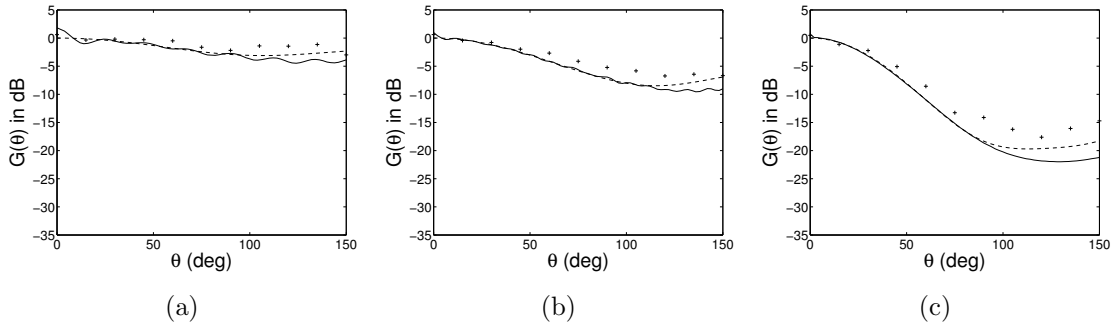


**Figure 4.** Comparison between numerical (solid), analytical predictions [1] (---) and experimental measurements [26] (+ + +) of the acoustic pressure directivity as a function of the angle in the absence of a mean flow: (a)  $ka = 0.74$ , (b)  $ka = 1.48$ , (c)  $ka = 2.96$ .

angle increases and the maximum differences are found to be at  $\theta = 150^\circ$ , i.e., -3.11 dB for  $ka = 0.74$ , -2.22 dB for  $ka = 1.48$  and -2.3 dB for  $ka = 2.96$ , respectively. For all three frequencies and for most angles, the analytical solution is located between the numerical and the experimental results.

For the case of a cold mean flow with a higher Mach number ( $M = 0.15$ ), the numerical results are compared with the theoretical prediction only, since no experimental results are available from Gorazd et al. for  $M = 0.15$ . The comparisons are depicted in Fig. 6. In general, good agreement is found for angles in the range  $30^\circ < \theta < 150^\circ$ . For most angles, the discrepancy from the theory is less than 3dB. The deviation of the simulation from the theoretical results is mainly found in the region of angles less than  $30^\circ$ . The smoothing of the curve representing the numerical results versus the analytical results in the region  $90^\circ < \theta < 120^\circ$  for the high frequency of  $ka = 3.77$ , as depicted in Fig. 6(d), might be due to the transfer of energy from the exciting chirp signal to higher-order modes, as discussed before.

An important feature of the directivity characteristics in the presence of a non-zero mean flow concerns the so-called “zone of relative silence”, where the sound wave in the vicinity of the axis is subject to additional attenuation. The result from the theoretical analysis of Savkar [37] and Munt [2] suggests that, for high frequencies and large Mach numbers, the zone of relative silence is so obvious that a cusp can be observed at  $\theta = \theta_s$  in the directivity pattern. Assuming that the medium outside the duct is stagnant and the speed of sound remains constant, the zone of relative silence is defined by [37]

$$\theta_s = \cos^{-1} \left( \frac{1}{1 + M} \right), \quad (14)$$

where  $M$  is the Mach number inside the duct.

Even for the low Mach number  $M = 0.036$ , the zone of relative silence ( $\theta_s = 15.15^\circ$ ) can be observed in both the experiments and the numerical results for  $ka = 2.96$ , as depicted in Fig. 5(c). For the case of higher Mach number  $M = 0.15$ , the zone of relative silence ( $\theta_s = 29.59^\circ$ ) are more obviously observed in the numerical results for all four

frequencies ( $ka = 0.74, 1.48, 2.96$  and  $3.77$ ).

However, we also observed that the numerical results demonstrates significant discrepancies compared to Gabard's model for the region of angles less than  $30^\circ$ . This might be either due to the effects of high viscosity of the LBM scheme or some unknown effects associated with the 2D axisymmetric LBM scheme, where the anti-symmetric higher modes can not be recovered, and some spurious 2D transversal modes might be generated per se. The modes below the cut off frequency die out exponentially as they propagate downstream and their contribution on the directivity is negligible, although some acoustic energy associated with these modes may find its way out of the pipe due to its reduced length. However, at values of  $ka$  above the first cut off frequency for plane modes ( $ka > 1.8$ ) the energy associated with transversal modes will propagate downstream and provide a significant contribution on the directivity pattern. This is evidenced in Fig. 6(c) and 6(d).

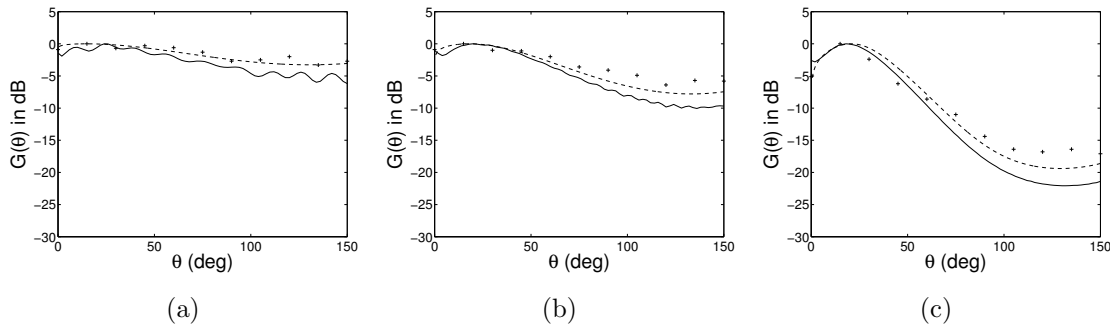


**Figure 5.** Comparison between numerical (solid), analytical [4] (- - -) predictions and experimental measurements [26] (+ + +) of the acoustic pressure directivity as a function of the angle in the presence of a mean flow at Mach = 0.036: (a)  $ka = 0.74$ , (b)  $ka = 1.48$ , (c)  $ka = 2.96$ .

## 4. Conclusions

In this paper, we presented a numerical technique based on an axisymmetric two-dimensional lattice Boltzmann scheme to predict the directivity pattern associated with the sound radiation at the open end of cylindrical ducts issuing a low Mach number cold subsonic jet into a stagnant fluid region.

The LBM scheme was first validated by comparing its results with the analytical model of Levine and Schwinger and experimental results of Gorazd et al. for the case of no flow. Then for the case of non-zero mean flow, the numerical results were compared with the theoretical prediction given by Gabard and Astley for Mach number  $M = 0.036$  and  $M = 0.15$  as well as experimental results obtained by Gorazd et al. for Mach number  $M = 0.036$ . Very good agreement was found with theoretical and experimental results for the case of no flow and the lower Mach number of  $M = 0.036$ . For the relatively higher Mach number of  $M = 0.15$ , the numerical result agrees very well with the theoretical prediction for angles greater than  $30^\circ$ , though significant discrepancies

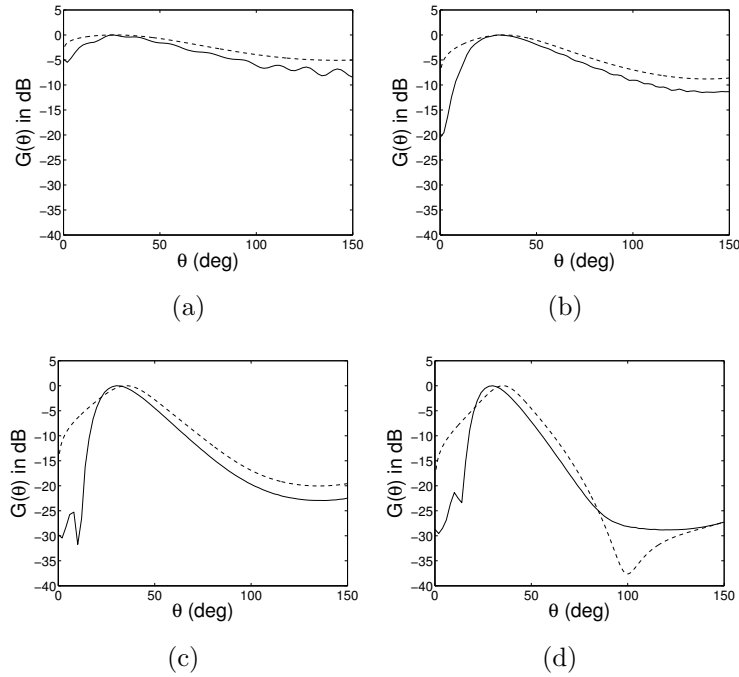


**Figure 6.** Comparison between numerical (solid) and analytical predictions [4] (- - -) of the acoustic pressure directivity as a function of the angle in the presence of a mean flow at Mach = 0.15: (a)  $ka = 0.74$ , (b)  $ka = 1.48$ , (c)  $ka = 2.96$ , (d)  $ka = 3.77$ .

are observed for angles less than  $30^\circ$ . The effects of the so-called zone of relative silence are clearly observed in the results of non-zero mean flow even for very low Mach number ( $M = 0.036$ ). This is interesting for some other cases, e.g., in the studies of musical acoustics, a woodwind instrument normally exhibits a very low Mach number flow.

The aforementioned discrepancies for the case of  $\theta < 30^\circ$  and  $M = 0.15$  are not well explained yet. For further investigations conducted by either experimental measurements or numerical simulations, some limitations might be considered. The theoretical model assumes an infinitely thin vortex sheet separating the jet and the neighboring quiescent fluid, which is not true for far field situations as well as the numerical simulations presented here. In addition, it was found in the numerical simulation presented here that the directivity pattern in directions close to the axis is very sensitive to the probing distance. Moreover, for better explaining the aforementioned smoothing effects demonstrated in the numerical results, we need more insight towards the axisymmetric D2Q9 model in terms of its capability of fully representing the higher radial modes, although the anti-axisymmetric circumferential modes are not supported for sure.

## Acknowledgements

The authors would like to thank Dr. Gwenael Gabard at University of Southampton, UK, for providing the numerical calculations of the theoretical model, and Mr. Lukasz

Gorazd and Dr. Anna Snakowska at AGH University of Science and Technology, Poland, for providing the experimental data. The second author wish to acknowledge funding from the CNPq for the grant “Chamada Universal/2012 - 472224”. We also wish to acknowledge funding from the Fonds québécois de la recherche sur la nature et les technologies (FQRNT), the Natural Sciences and Engineering Research Council of Canada (NSERC), and the Centre for Interdisciplinary Research in Music Media and Technology.

## References

- [1] H. Levine and J. Schwinger. On the radiation of sound from an unflanged circular pipe. *Phys. Rev.*, 73(4):383–406, 1948.
- [2] R. M. Munt. The interaction of sound with a subsonic jet issuing from a semi-infinite cylindrical pipe. *J. Fluid Mech.*, 83(4):609–640, 1977.
- [3] S. Rienstra. Acoustic radiation from a semi-infinite annular duct in a uniform subsonic mean flow. *J. of Sound and Vibration*, 94:267–288, 1984.
- [4] G. Gabard and R.J. Astley. Theoretical model for sound radiation from annular jet pipes: Far- and near-field solutions. *J. Fluid Mech.*, 549:315–341, 2006.
- [5] C.L. Rumsey, R.T. Biedron, and F. Farassat. Ducted-fan engine acoustic predictions using a navierstokes code. *J. of Sound and Vibration*, 213(4):643–664, 1998.
- [6] X. Zhang, X. Chen, C.L. Morfey, and P.A. Nelson. Computation of spinning modal radiation from an unflanged duct. *AIAA journal*, 42(9):1795–1801, 2004.
- [7] Y. Özyörük, E. Alpman, V. Ahuja, and L.N. Long. Frequency-domain prediction of turbofan noise radiation. *J. of Sound and Vibration*, 270(4):933–950, 2004.
- [8] X.X. Chen, X. Zhang, C.L. Morfey, and P.A. Nelson. A numerical method for computation of sound radiation from an unflanged duct. *J. of Sound and Vibration*, 270:573–586, 2004.
- [9] M. Hornikx, W. De Roeck, and W. Desmet. Simplified exhaust pipe noise radiation modelling using the fourier pstd method. In *International Conference on Noise and Vibration Engineering. Leuven, Belgium*, pages 20–22, 2010.
- [10] J.M. Buick, C.A. Greated, and D.M. Campbell. Lattice BGK simulation of sound waves. *EPL (Europhysics Letters)*, 43(3):235, 1998.
- [11] J.M. Buick, C.L. Buckley, C.A. Greated, and J. Gilbert. Lattice Boltzmann BGK simulation of nonlinear sound waves: the development of a shock front. *J. of Physics A: Mathematical and General*, 33:3917–3928, 2000.
- [12] P. L. Bhatnagar, E. P. Gross, and M. Krook. A model for collision processes in gases. I. Small amplitude processes in charged and neutral one-component systems. *Phys. Rev.*, 94(3):511, 1954.
- [13] J.M. Buick, M. Atig, D.J. Skulina, D.M. Campbell, J.P. Dalmont, and J. Gilbert. Investigation of non-linear acoustic losses at the open end of a tube. *The Journal of the Acoustical Society of America*, 129:1261, 2011.
- [14] E. M. Vigen. Viscously damped acoustic waves with the lattice Boltzmann method. *Philosophical Transactions of the Royal Society A: Mathematical, Physical and Engineering Sciences*, 369(1944):2246–2254, 2011.
- [15] E. M. Vigen. Acoustic multipole sources for the lattice Boltzmann method. *Phys. Rev. E*, 87(2):023306, 2013.
- [16] X.M. Li, R.C.K. Leung, and R.M.C. So. One-step aeroacoustics simulation using lattice Boltzmann method. *AIAA journal*, 44(1):78–89, 2006.
- [17] E.W.S. Kam, R.M.C. So, S.C. Fu, and R.C.K. Leung. Finite difference lattice boltzmann method applied to acoustic-scattering problems. *AIAA journal*, 48(2):354–371, 2010.

- [18] Y.B. Li and X.W. Shan. Lattice boltzmann method for adiabatic acoustics. *Philosophical Transactions of the Royal Society A: Mathematical, Physical and Engineering Sciences*, 369(1944):2371–2380, 2011.
- [19] P.T. Lew, L. Mongeau, and A. Lyrintzis. Noise prediction of a subsonic turbulent round jet using the lattice-boltzmann method. *The Journal of the Acoustical Society of America*, 128:1118, 2010.
- [20] K. Habibi, A. Najafi-Yazdi, P.T. Lew, and L. Mongeau. Simulation of sound radiated from turbulent heated jets using the lattice-boltzmann method. In *17th AIAA/CEAS Aeroacoustics Conference (32nd AIAA Aeroacoustics Conference) AIAA 2011-2844 5-8 June 2011, Portland, Oregon*, 2011.
- [21] A. R. da Silva and G. P. Scavone. Lattice Boltzmann simulations of the acoustic radiation from waveguides. *J. Phys. A: Math. Theor.*, 40:397–408, 2007.
- [22] A. R. da Silva, G. P. Scavone, and A. Lefebvre. Sound reflection at the open end of axisymmetric ducts issuing a subsonic mean flow: A numerical study. *J. of Sound and Vibration*, 327:507–528, 2009.
- [23] R. M. Munt. Acoustic transmission properties of a jet pipe with subsonic jet flow: I. The cold jet reflection coefficient. *J. of Sound and Vibration*, 142(3):413–436, 1990.
- [24] M.C.A.M. Peters, A. Hirschberg, A.J. Reijnen, and A.P.J. Wijnands. Damping and reflection coefficient measurements for an open pipe at low mach and low helmholtz numbers. *J. Fluid Mech.*, 256:499534, 1993.
- [25] S. Allam and M. Åbom. Investigation of damping and radiation using full plane wave decomposition in ducts. *J. of Sound and Vibration*, 292(3-5):519534, 2002.
- [26] L. Gorazd, J. Jurkiewicz, and A. Snakowska. Experimental verification of the theoretical model of sound radiation from an unflanged duct with low mean flow. *Archives of Acoustics*, 37(2):227–236, 2012.
- [27] I. Halliday, L. A. Hammond, C. M. Care, K. Good, and A. Stevens. Lattice Boltzmann equation hydrodynamics. *Phys. Rev. E.*, 64(011208):1–8, 2001.
- [28] Y.H. Qian, D. d’Humières, and P. Lallemand. Lattice BGK models for Navier-Stokes equation. *Europhysics Letters*, 17(6):479–484, 1992.
- [29] X.D. Niu, C. Shu, and Y.T. Chew. An axisymmetric lattice Boltzmann model for simulation of Taylor–Couette flows between two concentric cylinders. *International Journal of Modern Physics C*, 14(06):785–796, 2003.
- [30] T.S. Lee, H.B. Huang, and C. Shu. An axisymmetric incompressible lattice BGK model for simulation of the pulsatile flow in a circular pipe. *International Journal for Numerical Methods in Fluids*, 49(1):99–116, 2005.
- [31] X.Y. He and L.S. Luo. Lattice Boltzmann model for the incompressible Navier–Stokes equation. *J. of Statistical Physics*, 88(3-4):927–944, 1997.
- [32] D. A. Wolf-Gladrow. *Lattice Gas Cellular Automata and Lattice Boltzmann Models: An Introduction. Lecture Notes in Mathematics*. Springer, Berlin / Heidelberg, 2004.
- [33] E.W.S. Kam, R.M.C. So, and R.C.K. Leung. Non-reflecting boundary conditions for one-step LBM simulation of aeroacoustics. In *27th AIAA Aeroacoustics Conference, 8-10 May 2006, Cambridge, Massachusetts*, 2006.
- [34] M. Bouzidi, M. Firdaouss, and P. Lallemand. Momentum transfer of a Boltzmann-lattice fluid with boundaries. *Physics of Fluids*, 13(11):3452, 2001.
- [35] P. Lallemand and L.S. Luo. Lattice Boltzmann method for moving boundaries. *J. of Computational Physics*, 184:406–421, 2003.
- [36] S. Succi. *The lattice Boltzmann equation for fluid dynamics and beyond*. Oxford University Press, 2001.
- [37] S. D. Savkar. Radiation of cylindrical duct acoustic modes with flow mismatch. *J. of Sound and Vibration*, 42(3):363–386, 1975.